



## ORIGINAL ARTICLE

# Effect of copper source on the structure–activity of $\text{CuAl}_2\text{O}_4$ spinel catalysts for CO hydrogenation



Lusheng Shi, Pengquan Yan, Zhihua Gao<sup>\*</sup>, Wei Huang

State Key Laboratory of Clean and Efficient Coal Utilization, Taiyuan University of Technology, Taiyuan 030024, Shanxi, China

Received 21 August 2022; accepted 21 November 2022

Available online 26 November 2022

## KEYWORDS

$\text{CuAl}_2\text{O}_4$ ;  
CO hydrogenation;  
Slurry reactor;  
Catalyst;  
Higher alcohols;  
Dimethyl ether

**Abstract** Due to the complexity of the structure–activity relationship of the  $\text{CuAl}_2\text{O}_4$  spinel catalyst, optimization of the catalyst structure is a great challenge. In this paper, three different  $\text{CuAl}_2\text{O}_4$  spinel catalysts were prepared by the solid-phase method using copper hydroxide, copper nitrate, and copper oxide as the copper source, respectively, to study the difference in the structure of  $\text{CuAl}_2\text{O}_4$  spinel catalysts induced by the raw materials and the catalytic behavior for CO hydrogenation. The structure of  $\text{CuAl}_2\text{O}_4$  spinel catalyst was characterized by XRD, BET, SEM, TEM,  $\text{H}_2$ -TPR and XPS. The activity of CO hydrogenation over the  $\text{CuAl}_2\text{O}_4$  spinel catalyst without pre-reduction was evaluated in the slurry reactor. The results demonstrated that different copper sources had obvious influence on the  $\text{CuAl}_2\text{O}_4$  spinel texture properties, surface enrichment degree, as well as decomposition and reduction ability, which further regulated the ratio of  $\text{Cu}^+/\text{Cu}^0$  and thus affected the catalytic performance, especially the alcohol distribution. The  $\text{CuAl}_2\text{O}_4$  spinel, employing copper hydroxide as the copper source, showed better selectivity of  $\text{C}_2+\text{OH}$ , which was assigned to a higher ratio of  $\text{Cu}^+/\text{Cu}^0$ , along with larger pore size and pore volume. Moreover, the synergistic effect between  $\text{Cu}^0$  and  $\gamma\text{-Al}_2\text{O}_3$  improved the selectivity of dimethyl ether.

© 2022 The Author(s). Published by Elsevier B.V. on behalf of King Saud University. This is an open access article under the CC BY-NC-ND license (<http://creativecommons.org/licenses/by-nc-nd/4.0/>).

## 1. Introduction

$\text{CuAl}_2\text{O}_4$  spinel has a face-centered cubic crystal structure, in which  $\text{Cu}^{2+}$  is occupied a tetrahedral position and is stable

in the oxide lattice structure (Sickafus et al., 1999, Yong et al., 2013, Wang et al., 2017). The active Cu species with high dispersion were gradually released from  $\text{CuAl}_2\text{O}_4$  spinel during the reaction, thereby avoiding the agglomeration and rapid sintering of Cu species (Maiti et al., 2016, Wan et al., 2016, Li et al., 2018). Catalytic conversion of C1 molecules is a vitally important process because of its close correlation to energy and environmental implications (Liu et al., 2020a, Altass et al., 2021, Salama et al., 2021a, 2021b, Altass et al., 2022). It was reported that  $\text{CuAl}_2\text{O}_4$  spinel catalyst showed excellent catalytic performance in C1 catalysis, such as methanol steam reforming (Xi et al., 2014, Liu et al., 2022a, 2022b),

<sup>\*</sup> Corresponding author.

E-mail addresses: [slsynl@163.com](mailto:slsynl@163.com) (L. Shi), [gaozhihua@tyut.edu.cn](mailto:gaozhihua@tyut.edu.cn) (Z. Gao).

Peer review under responsibility of King Saud University.



reverse water gas shift (Bahmanpour et al., 2019), and CO oxidation reaction (Severino et al., 1998).

Our group (Huang et al., 2011, Liu et al., 2020b, Liu et al., 2022a, 2022b) had been engaged in the research of CO hydrogenation in the slurry reactor over the Cu-Zn-Al slurry catalyst for more than two decades, which was prepared by our independently developed catalyst preparation technology-complete liquid-phase method. The novelty of this method was that the catalyst precursor was directly heat-treated in an inert medium to obtain the slurry without conventional drying and calcination procedures. So-prepared Cu-Zn-Al slurry catalyst showed excellent activity and stability for CO hydrogenation to higher alcohols ( $C_{2+}OH$ ) or dimethyl ether. In our previous work, Deng et al. (Deng et al., 2019) explored the influence of heat treatment pressure on the catalytic performance in CO hydrogenation over Cu-Zn-Al slurry catalyst. Compared with the constant pressure, the catalyst heat-treated under 1.0 MPa exhibited excellent catalytic performance with the higher alcohols mass fraction in total alcohols, increased from 25.8 % to 65.9 %, which was ascribed to the formation of  $CuAl_2O_4$  spinel phase. But it was difficult to control the  $CuAl_2O_4$  spinel structure in Cu-Zn-Al slurry catalysts through the complete liquid-phase method. To further investigate the structure change and catalytic performance of  $CuAl_2O_4$  spinel, Yan et al. (Yan et al., 2021) in our group designed to fabricate  $CuAl_2O_4$  spinel *via* traditional preparation methods (such as solid-phase method, sol-gel method, citric acid method, and co-precipitation method), and the spinel was directly added into the slurry reactor for CO hydrogenation without reduction. The results disclosed that the  $CuAl_2O_4$  spinel obtained by the solid-phase method favored the production of higher alcohols.

Our former study found that the preparation method had a remark influence on the structure and catalytic performance of  $CuAl_2O_4$  spinel. But the specific relationship between the  $CuAl_2O_4$  structure and the activity for CO hydrogenation remained unclear. It was therefore of supreme importance to tune the structure of  $CuAl_2O_4$  spinel. As we known, the synthetic method was one factor to affect catalyst structure (Alshorifi et al., 2021, El-Hakam et al., 2022). Besides,  $CuAl_2O_4$  spinel synthesis parameters, including Cu/Al molar ratio, calcination atmosphere, and introducing the third components, showed significant influence on its structure (Liu et al., 2020c, Liu et al., 2022c). So, in this paper, the  $CuAl_2O_4$  spinel catalysts were synthesized by the solid-phase method employing copper hydroxide, copper nitrate, and copper oxide as the copper source, respectively. We attempted to explore the difference in the structure of  $CuAl_2O_4$  spinel induced by the copper sources and the catalytic behavior for CO hydrogenation and to develop the structure-activity relationship.

## 2. Experimental

### 2.1. Materials

$Cu(NO_3)_2 \cdot 3H_2O$ , liquid paraffin and petroleum ether were obtained from Tianjin Kemiou Chemical Reagent Co., Ltd., China. Pseudo-boehmite, CuO and  $Cu(OH)_2$  were purchased from Shanghai Aladdin Biochemical Technology Co., Ltd., China. All chemical reagents were analytical grade and used without further purification. CO,  $H_2$ ,  $N_2$ , Ar and He, with

purities of 99.99 %, were provided by the Product of Taiyuan Fujiang Special Gas Co., Ltd., China.

### 2.2. Catalyst preparation

The Cu and Al raw materials with Cu/Al = 1/2(molar ratio) were well mixed and ball-milled by a planetary ball mill for 6 h. The powder was calcined in the air atmosphere at 900 °C for 3 h. The aluminum source was pseudo-boehmite. Copper hydroxide, copper nitrate, and copper oxide were selected as the copper source, respectively. The corresponding  $CuAl_2O_4$  catalysts were denoted as So-OH, So-NO, and So-O, respectively.

### 2.3. Catalyst characterization

Before characterization, the  $CuAl_2O_4$  spinel slurry catalyst after the reaction was centrifuged, extracted with petroleum ether for 4 days to remove the residual liquid paraffin, and then naturally dried to obtain a solid sample.

The crystal phase structure was characterized by DX-2700 X-ray diffraction apparatus (Dandong Fangyuan Instrument Co., Ltd.) with Cu  $K\alpha$  source ( $\lambda = 0.1546$  nm) with voltage and current at 40 kV and 30 mA, respectively. The sample was scanned over the range of 5–85° at a scanning rate of 8°/min to identify the crystalline structure. The crystallite size of  $CuAl_2O_4$  spinel catalyst was calculated using the Scherrer formula.

The texture parameter was measured by a QDS-30 physical adsorption instrument (Quantachrome Company, USA) using  $N_2$  as adsorbate at -196 °C. Prior to the test, the sample was pretreated under vacuum at 200 °C for 4 h to remove the adsorbed impurities. The specific surface area was determined by the BET (Brunauer-Emmett-Teller) method, and the most probable pore size and pore volume were obtained by the BJH (Barret-Joyner-Halenda) method.

Scanning electron microscopy (SEM) was performed using JSM-6010PLUS/LV emission electron microscope. The samples were observed at an accelerating voltage of 20 kV and sputter-coated for 120 s in a sputter coated fitted with Au before testing.

The transmission electron microscope (TEM) image was determined by the JEM-2100 instrument (Japan JEOL company) with an accelerating voltage of 300 kV. Samples were dispersed in alcohol in an ultrasonic bath, and a drop of the supernatant suspension was poured onto a holey carbon-coated grid and dried completely before the measurements.

Hydrogen temperature-programmed reduction ( $H_2$ -TPR) was measured in a chemisorption instrument (TP-5080, Tianjin Xianquan Corporation). 50 mg catalyst was pre-heated at 150 °C for 0.5 h under He flow and then cooled to 50 °C. Afterwards, the reduction process was recorded with the temperature ramping up from 50 °C to 800 °C at 10 °C·min<sup>-1</sup> under a 5 %  $H_2/N_2$  flow of 30 mL·min<sup>-1</sup>. The hydrogen consumption signal was recorded using a thermal conductivity detector (TCD).

X-ray photoelectron spectroscopy (XPS) data was performed on an ESCALAB 250Xi spectrometer (American Thermo Fischer Company) equipped with Al  $K\alpha$  radiation ( $h\nu = 1486.6$  eV). The binding energies of Cu 2p and CuLMM were calibrated by the C 1 s peak ( $BE = 284.8$  eV).

## 2.4. Catalyst activity evaluation

CO hydrogenation over different CuAl<sub>2</sub>O<sub>4</sub> spinel catalysts was evaluated in a 500 mL slurry reactor with a continuous mechanical agitator. Firstly, the prepared CuAl<sub>2</sub>O<sub>4</sub> spinel was uniformly dispersed in 300 mL of liquid paraffin (solid holdup 10 %), and did not need to be reduced. Then, the reaction was carried out by feeding syngas (H<sub>2</sub>/CO = 2) at a flow rate of 150 mL·min<sup>-1</sup>. The reaction pressure and temperature were 4 MPa and 280 °C, respectively. The steady-state activity measurement was taken after at least 24 h on the stream, and the reaction was continuously evaluated for six days. The H<sub>2</sub>, CO and CO<sub>2</sub> in the gas phase products were detected by thermal conductivity detectors (TCD, TDX-01). Hydrocarbons, alcohols and dimethyl ether were detected by a flame ionization detector (FID, HP-PLOT/Q). The liquid phase product was condensed and collected daily, and analyzed by the FID detector. The carbon balance ( $\varepsilon_C$ ) was determined according to Eq. (1). The CO conversion ( $X_{CO}$ ) and product selectivity ( $S_i$ ) were calculated after carbon balance according to Eqs. (2) and (3), respectively.

$$\varepsilon_C = \frac{\sum n_i(g) + \sum n_i(l)}{n(CO)_{in}} \times 100\% \quad (1)$$

$$X_{CO} = \frac{\sum n_i(g) + \sum n_i(l)}{n(CO)_{out} + \sum n_i(g) + \sum n_i(l)} \times 100\% \quad (2)$$

$$S_i = \frac{n_i(g) + n_i(l)}{\sum n_i(g) + \sum n_i(l)} \times 100\% \quad (3)$$

Where ( $\varepsilon_C$ ) was the carbon balance;  $X_{CO}$  was the conversion of CO (C-mol%);  $S_i$  was the selectivity of component  $i$  (C-mol %);  $i$  was all C-containing compounds except CO in the gas and liquid products;  $n(CO)_{in}$  was the amount of CO in the inlet gas (mol);  $n(CO)_{out}$  was the amount of CO in the outlet gas (mol);  $n_i(g)$  and  $n_i(l)$  was the carbon atom of component  $i$  in the outlet gas (mol) and liquid phase product (mol), respectively.

## 3. Results and discussion

### 3.1. XRD characterization

Fig. 1 showed the XRD patterns of different CuAl<sub>2</sub>O<sub>4</sub> spinels. Before the reaction (Fig. 1a), the apparent diffraction peaks were observed in all catalysts at  $2\theta = 31.29^\circ, 36.87^\circ, 44.84^\circ, 55.70^\circ, 59.40^\circ, 65.29^\circ, 74.18^\circ$  and  $77.41^\circ$ , which were attributed to CuAl<sub>2</sub>O<sub>4</sub> spinel (PDF No.71–0967). Moreover, So-NO and So-O catalysts showed CuO diffraction peaks at  $2\theta = 35.72^\circ$  and  $38.96^\circ$  (PDF No.48–1548). The appearance of CuO was ascribed to the fact that part of Cu<sup>2+</sup> did not enter into the interstices of spinel and existed as free CuO. As for the So-OH catalyst, no CuO diffraction peaks appeared, and the diffraction peaks intensity of CuAl<sub>2</sub>O<sub>4</sub> spinel was the weakest among the three catalysts. It was indicated that copper hydroxide as the copper source was conducive to the oxidation of copper hydroxide and pseudo-boehmite during the process of calcination, and then the corresponding oxides formed CuAl<sub>2</sub>O<sub>4</sub> spinel with higher purity through the solid–solid interaction (Luo et al., 2005, Xi et al., 2013). The average crystallite sizes of CuAl<sub>2</sub>O<sub>4</sub> spinel catalysts before the reaction, calculated by the Scherrer equation, were listed in Table 1. It can be founded that the change of copper source had no obvious effect on the crystallite size of CuAl<sub>2</sub>O<sub>4</sub> spinel catalysts.

After the reaction (Fig. 1b), the characteristic diffraction peaks of CuAl<sub>2</sub>O<sub>4</sub> disappeared, whereas that of Cu<sup>0</sup> and  $\gamma$ -Al<sub>2</sub>O<sub>3</sub> appeared, indicating that the CuAl<sub>2</sub>O<sub>4</sub> was decomposed and reduced to low valence copper species and  $\gamma$ -Al<sub>2</sub>O<sub>3</sub> during the CO hydrogenation reaction at 280 °C and 4 MPa (Feng et al., 2009, Arjmand et al., 2012). It was worth noting that only the So-OH catalyst showed obvious Cu<sub>2</sub>O diffraction peaks at  $2\theta = 36.52^\circ, 42.42^\circ$ , and  $61.55^\circ$  (PDF No.05–0667), suggesting that the different copper sources influenced the decomposition and reduction properties of CuAl<sub>2</sub>O<sub>4</sub> spinel catalyst.

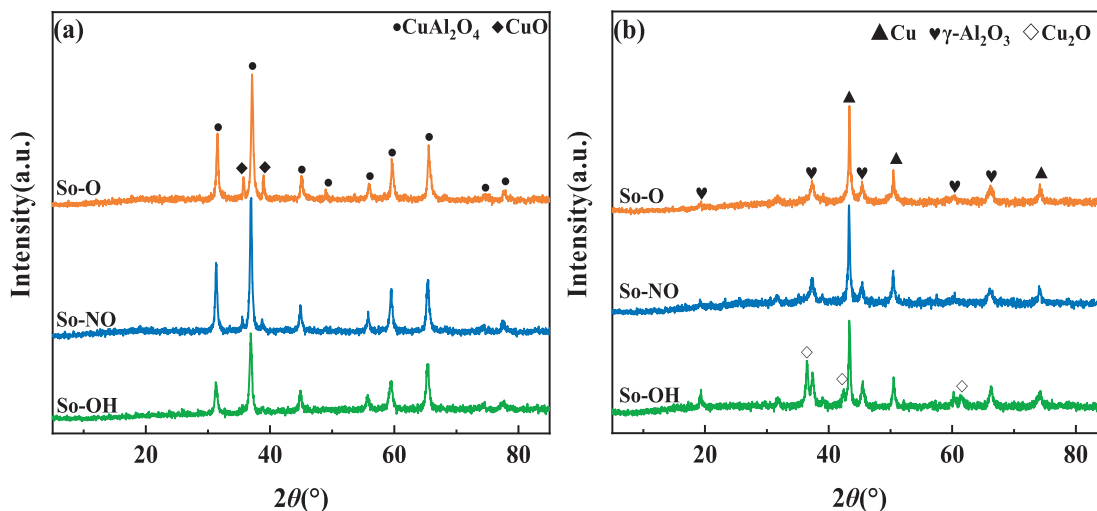


Fig. 1 XRD patterns of different CuAl<sub>2</sub>O<sub>4</sub> spinel before (a) and after (b) the reaction.

**Table 1** Texture properties of different  $\text{CuAl}_2\text{O}_4$  spinel before and after the reaction.

Sample	Before reaction <sup>a</sup>			After reaction <sup>a</sup>			$d_{\text{CuAl}_2\text{O}_4}(\text{nm})^b$
	$S_{\text{BET}}$	$V_{\text{P}}$	$D_{\text{P}}$	$S_{\text{BET}}$	$V_{\text{P}}$	$D_{\text{P}}$	
So-OH	19.2	0.15	30.3	20.8	0.12	30.2	20.6
So-NO	18.7	0.07	9.5	19.2	0.06	9.6	23.6
So-O	31.0	0.10	9.5	33.0	0.09	7.8	22.6

<sup>a</sup> The specific surface area  $S_{\text{BET}}(\text{m}^2/\text{g})$ , the pore volume  $V_{\text{P}}(\text{cm}^3/\text{g})$  and the most probable pore size  $D_{\text{P}}(\text{nm})$  are calculated by  $\text{N}_2$  physical adsorption.

<sup>b</sup> The crystallite size of the spinel phase was calculated from the average value of the full-width at half-maximum (FWHM) of  $\text{CuAl}_2\text{O}_4$  (220), (311), (400), (422), (511), (440) diffraction peaks by means of the Scherer formula.

### 3.2. $\text{N}_2$ adsorption–desorption characterization

Fig. 2 displayed the  $\text{N}_2$  adsorption–desorption curves and pore size distribution of  $\text{CuAl}_2\text{O}_4$  spinel before and after the reaction. The existence of a typical IV isotherm indicated that the catalysts preserved a uniform mesoporous structure

(Salama et al., 2021a, 2021b). However, the shapes of hysteresis loops were somewhat different, implying various porous structures. The isotherm of the So-OH catalyst displayed H3-type hysteresis loop, indicating the existence of slit pores. In contrast, hysteresis loops for So-NO and So-O catalysts were H4-type, which was attributed to the narrow fissure hole.

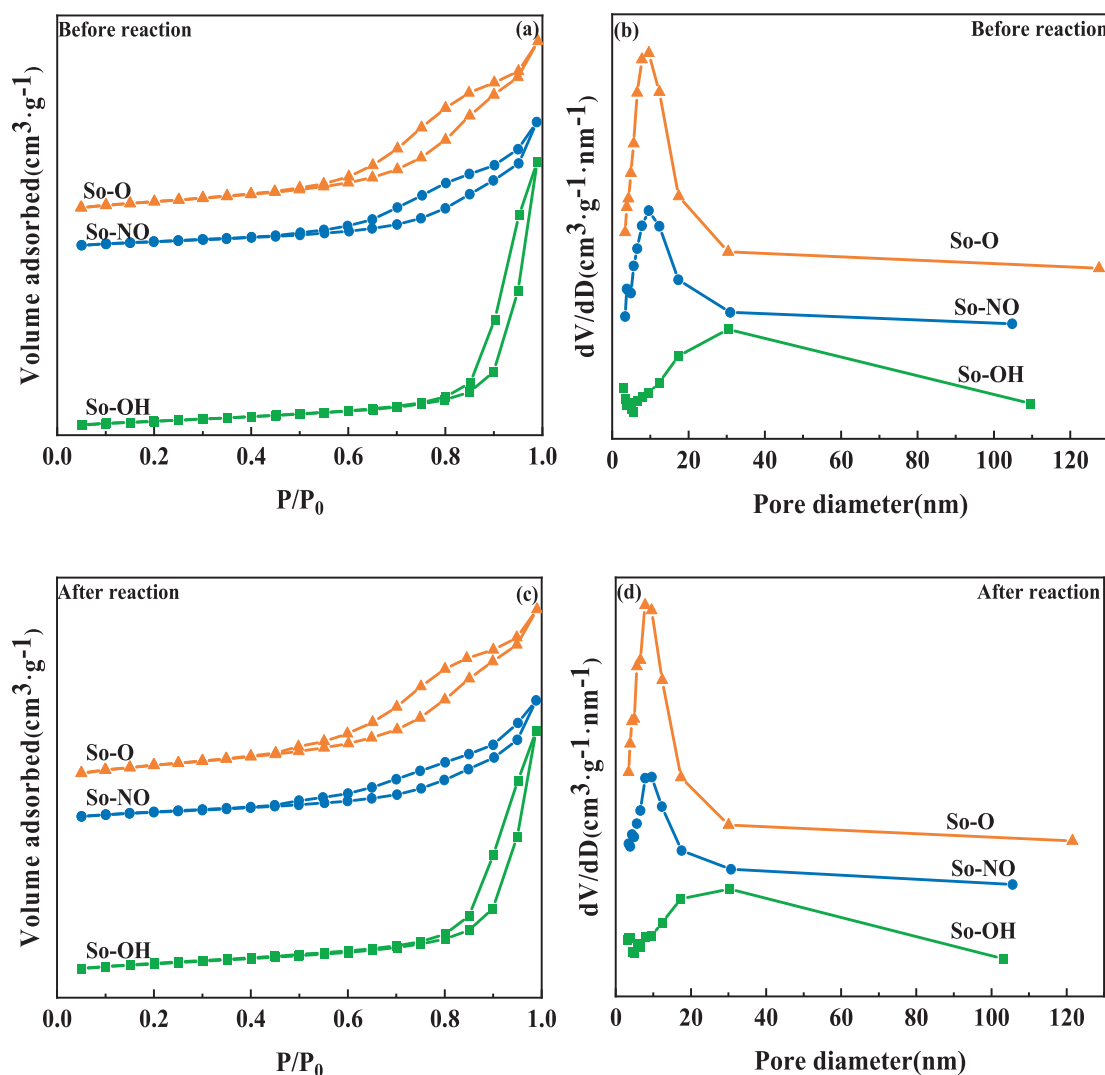


**Fig. 2**  $\text{N}_2$  absorption–desorption curves and pore size distribution of  $\text{CuAl}_2\text{O}_4$  spinel before (a, b) and after (c, d) the reaction.

As presented in Table 1, The specific surface area of the catalysts decreased in the following order: So–O > So–OH > So–NO. The pore volume and the most probable pore size of the So–OH catalyst were maximum, reaching 0.15 cm<sup>3</sup>·g<sup>-1</sup> and 30.3 nm, respectively, whereas those of So–NO and So–O catalysts were similar, and their most probable pore size was only 1/3 of So–OH. The results showed that copper sources had a significant impact on the texture properties. After the reaction, the texture properties of all catalysts remained almost unchanged, indicating that the pore structure of catalysts was steady during the reaction.

### 3.3. SEM characterization

Fig. 3 showed SEM images of different CuAl<sub>2</sub>O<sub>4</sub> spinel catalysts before the reaction. It can be seen that the dispersion of the three catalysts was significantly different. The So–OH catalyst was homogeneously distributed with slightly agglomerated, and the particle size was mainly less than 3 μm. The agglomeration of the So–NO catalyst was severe with large particles (> 10 μm). The So–O catalyst was homogeneous and uniform with small particles (≤ 3 μm).

Fig. 4 exhibited SEM images of different CuAl<sub>2</sub>O<sub>4</sub> spinel catalysts after the reaction. The particle size of the So–OH and So–O catalysts increased after reaction due to the slight sintering of the Cu<sup>0</sup> particles during the reaction process. However, the particle size of the So–NO catalyst decreased and the dispersion improved after reaction. It was speculated that this phenomenon may be related with the decomposition of seriously agglomerated CuAl<sub>2</sub>O<sub>4</sub> spinel during the reaction, which could gradually release high dispersion Cu species (Maiti et al., 2016, Wan et al., 2016, Li et al., 2018, Liu et al., 2022a, 2022b).

### 3.4. TEM characterization

TEM images of different CuAl<sub>2</sub>O<sub>4</sub> spinel catalysts before the reaction were shown in Fig. 5. All catalysts were stacked in irregular flakes. The diameter of So–OH [Fig. 5(a)] and So–NO [Fig. 5(b)] catalysts were mainly distributed in the range of 20 ~ 30 nm. Moreover, their accumulation was relatively thin, and individual flakes can be observed. However, the diameter of the So–O catalyst was small and primarily within 10 ~ 15 nm. Compared with So–OH and So–NO catalysts, its accumulation was thick, and no single flakes appeared [Fig. 5(c)], which was consistent with the SEM result that the So–O catalyst was uniformly dispersed with small particles.

In the HRTEM, the So–OH catalyst [Fig. 5(a')] exhibited 0.24 nm and 0.28 nm lattice spaces, which was ascribed to CuAl<sub>2</sub>O<sub>4</sub>(311) and CuAl<sub>2</sub>O<sub>4</sub>(220) facet, respectively (Ding et al., 2009). However, the So–NO [Fig. 5(b')] and So–O [Fig. 5(c')] catalysts only presented a lattice space of 0.28 nm, indicating that the copper source affected the facets exposure of CuAl<sub>2</sub>O<sub>4</sub> spinel.

### 3.5. H<sub>2</sub>-TPR characterization

Fig. 6(a) displayed the H<sub>2</sub>-TPR profiles of different CuAl<sub>2</sub>O<sub>4</sub> spinel catalysts before the reaction. Three reduction peaks were observed and named as α<sub>1</sub> (170–220 °C), α<sub>2</sub> (225–280 °C), and β (290–470 °C), respectively. According to the above XRD characterization, α<sub>1</sub> was ascribed to the reduction

of highly dispersed free CuO species, α<sub>2</sub> was assigned to the reduction of free CuO species with large crystallite size, and β was attributed to the reduction of CuAl<sub>2</sub>O<sub>4</sub> (Luo et al., 2005, Kwak et al., 2012, Hou et al., 2021). The molar percentage of CuO in all copper species [CuO/(CuO + CuAl<sub>2</sub>O<sub>4</sub>)] calculated according to the reduction peak area ratio in the H<sub>2</sub>-TPR spectra were 15.0 %, 30.5 % and 24.9 % for the So–OH, So–NO and So–O catalysts, respectively (See Table 2). The amount of CuO in the So–OH catalyst was the least among the three catalysts. No CuO diffraction peaks were observed in XRD characterization, indicating that CuO was highly dispersed or amorphous. Meanwhile, it can be founded that the molar percentage of CuAl<sub>2</sub>O<sub>4</sub> in all copper species [CuAl<sub>2</sub>O<sub>4</sub>/(CuO + CuAl<sub>2</sub>O<sub>4</sub>)] was 85 %, 69.5 %, and 75.1 % in the So–OH, So–NO, and So–O catalysts, respectively, indicating that the copper sources showed obvious influence on the purity of the CuAl<sub>2</sub>O<sub>4</sub> spinel.

The H<sub>2</sub>-TPR spectra of different CuAl<sub>2</sub>O<sub>4</sub> spinel catalysts after the reaction were shown in Fig. 6(b). Compared with the catalysts before the reaction, the reduction peak of CuAl<sub>2</sub>O<sub>4</sub> spinel around 360 °C disappeared, and the peak area of about 200 °C obviously increased, indicating that the CuAl<sub>2</sub>O<sub>4</sub> spinel was decomposed and reduced during the reaction. Agzamova et al. reported that CuAl<sub>2</sub>O<sub>4</sub> spinel could decompose to produce CuO and Al<sub>2</sub>O<sub>3</sub> at 6 MPa, 800 °C (Agzamova et al., 2020). In this work, based on XRD results, the CuAl<sub>2</sub>O<sub>4</sub> spinel decomposed at 4 MPa, 280 °C because the reaction atmosphere (CO + H<sub>2</sub>) could accelerate the decomposition. In order to distinguish from free CuO, the CuO produced by the CuAl<sub>2</sub>O<sub>4</sub> spinel decomposition was named as the released CuO. Our previous work reported that CuO would be completely reduced to Cu after heat-treated in liquid paraffin at 280 °C for 1 h (Fan et al., 2013). Based on this result, it was reasonable to assume that free CuO in the CuAl<sub>2</sub>O<sub>4</sub> spinel catalysts was reduced to Cu during 144 h reaction at 280 °C in liquid paraffin.

After peak fitting of Fig. 6(b), the reduction peaks around 200 °C can be classified into three peaks. Peak I belonged to the reduction of the released CuO. Compared with the reduction of free CuO before the reaction, it could be seen that, after the reaction, the reduction temperature of the released CuO was shifted to a lower temperature, implying there existed a difference between the structure of free CuO and released CuO. It was reported that the CuAl<sub>2</sub>O<sub>4</sub> spinel gradually released CuO during the reaction, and the released CuO had high dispersion and could avoid agglomeration (Maiti et al., 2016, Wan et al., 2016, Li et al., 2018, Liu et al., 2022a, 2022b). Further studies will be needed to obtain the precise difference between the structure of free CuO and the released CuO. Moreover, it can be seen from Fig. 6(b) that peak I did not appear for the So–OH catalyst, indicating the released CuO could be further reduced to low valence copper species. According to the XRD patterns [Fig. 1(b)] and Cu LMM spectra [Fig. 7(c)], there existed Cu<sub>2</sub>O and Cu for So–OH catalyst after the reaction. Hence, peak II was assigned to the reduction of highly dispersed Cu<sub>2</sub>O, and peak III corresponded to the reduction of Cu<sub>2</sub>O with a good crystallite shape. It can be founded that the reduction peaks of the released CuO and highly dispersed Cu<sub>2</sub>O appeared for the So–NO and So–O catalysts. As for the So–OH catalysts, the reduction peak of the released CuO disappeared, and the reduction peaks of the highly dispersed Cu<sub>2</sub>O and crystalline Cu<sub>2</sub>O appeared, illustrating that CuO released by the CuAl<sub>2</sub>O<sub>4</sub> spinel decomposi-

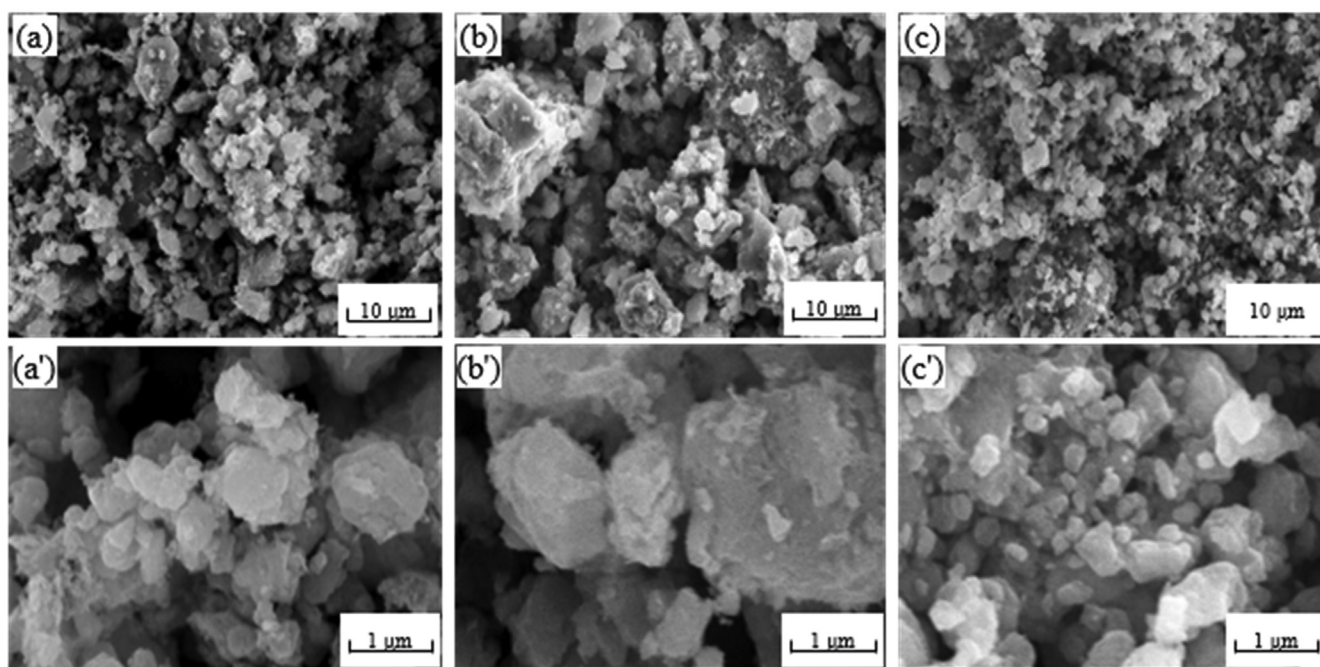


Fig. 3 SEM images of different  $\text{CuAl}_2\text{O}_4$  spinel before the reaction. (a, a') So-OH; (b, b') So-NO; (c, c') So-O.

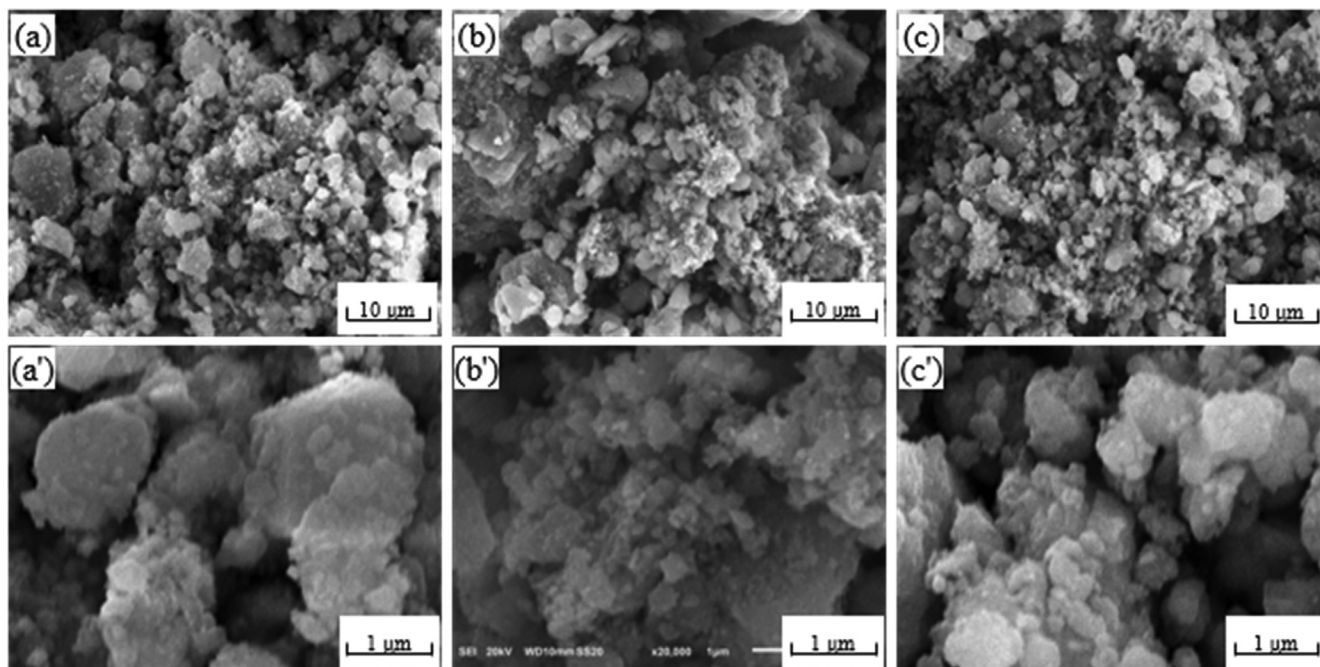


Fig. 4 SEM images of different  $\text{CuAl}_2\text{O}_4$  spinel after the reaction (a, a') So-OH; (b, b') So-NO; (c, c') So-O.

tion was rapidly reduced. Hence, it can be concluded that the  $\text{CuAl}_2\text{O}_4$  spinel prepared by different copper sources possessed various decomposition and reduction abilities during the reaction. Specifically, the So-OH catalyst with the highest purity of  $\text{CuAl}_2\text{O}_4$  promoted the released  $\text{CuO}$  in the bulk phase completely reduced to low valence copper species, and  $\text{Cu}_2\text{O}$  with good crystallization appeared. While catalysts with lower purity of  $\text{CuAl}_2\text{O}_4$  resulted in part of the released  $\text{CuO}$  not being timely reduced and no crystalline  $\text{Cu}_2\text{O}$  formed.

### 3.6. XPS characterization

To further explore the changes in the chemical valence state and existing forms of the elements over the catalyst surface before and after the reaction, the catalysts were characterized by XPS. As shown in Fig. 7(a), all catalysts before the reaction displayed shake-up satellite peaks between 941 ~ 943 eV, indicating the existence of  $\text{Cu}^{2+}$  on the catalyst surface. After peak

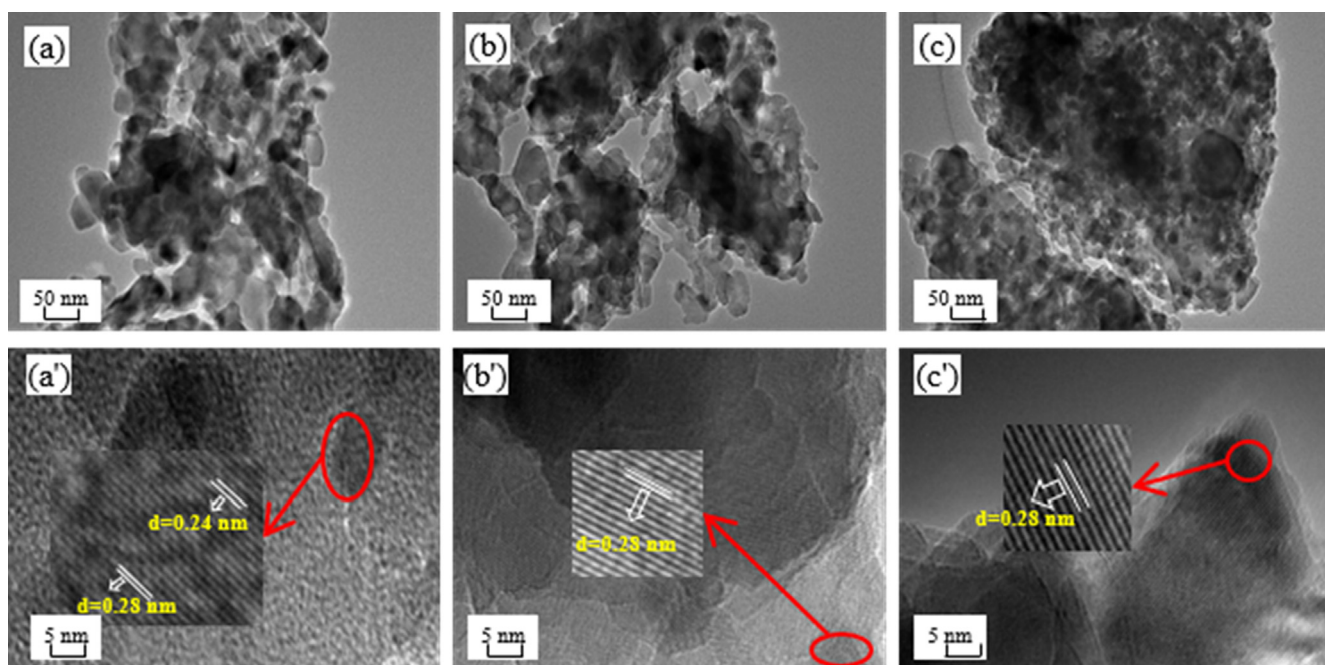


Fig. 5 TEM and HRTEM images of different  $\text{CuAl}_2\text{O}_4$  spinel before the reaction. (a, a') So-OH; (b, b') So-NO; (c, c') So-O.

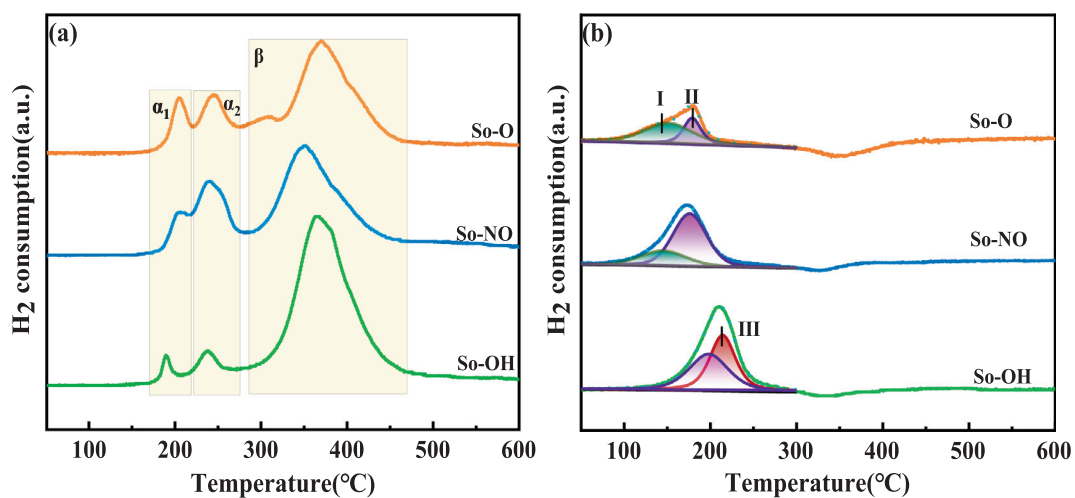


Fig. 6  $\text{H}_2$ -TPR profiles of different  $\text{CuAl}_2\text{O}_4$  spinel before (a) and after (b) the reaction.

**Table 2** The molar percentage of different copper species.

Catalyst	Before reaction(bulk) <sup>a</sup>		Before reaction(surface) <sup>b</sup>		After reaction <sup>c</sup>	
	CuO(%)	$\text{CuAl}_2\text{O}_4$ (%)	CuO(%)	$\text{CuAl}_2\text{O}_4$ (%)	$\text{Cu}^+$ (%)	$\text{Cu}^0$ (%)
So-OH	15.0	85.0	23.4	76.6	93.1	6.9
So-NO	30.5	69.5	31.0	69.0	91.4	8.6
So-O	24.9	75.1	58.9	41.1	83.5	16.5

<sup>a</sup> The data was calculated by the reduction peak area ratio in the  $\text{H}_2$ -TPR before reaction.

<sup>b</sup> The data was obtained by the peak area ratio of Cu  $2p_{3/2}$  before reaction.

<sup>c</sup> The data was acquired by the peak area ratio of Cu LMM.

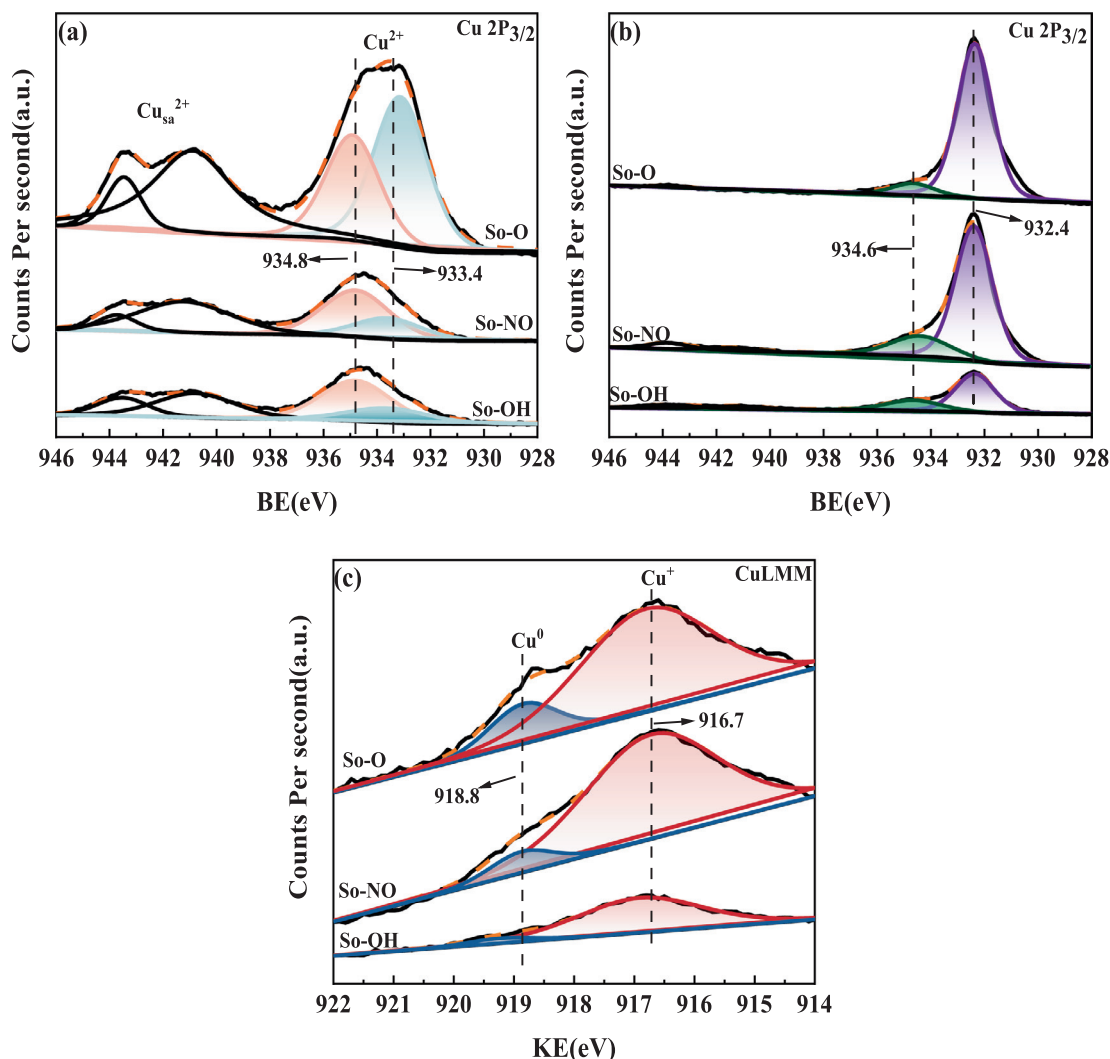


Fig. 7 XPS spectra of different  $\text{CuAl}_2\text{O}_4$  spinel before (a) and after (b, c) the reaction.

fitting, the binding energies of  $\text{Cu } 2p_{3/2}$  located at 934.8 eV and 933.4 eV were attributed to  $\text{CuAl}_2\text{O}_4$  and  $\text{CuO}$ , respectively (Severino et al., 1998). The molar percentage of  $\text{CuAl}_2\text{O}_4$  on the catalyst surface calculated by the area ratio of  $\text{Cu } 2p_{3/2}$  followed the order:  $\text{So-OH} > \text{So-NO} > \text{So-O}$  (See Table 2). Moreover, compared with the molar percentage of  $\text{CuAl}_2\text{O}_4$  in catalyst bulk, that of  $\text{CuAl}_2\text{O}_4$  on the catalyst surface over the  $\text{So-OH}$  and  $\text{So-O}$  catalysts decreased by 8.4 % and 34.0 %, respectively. But the molar percentage of the  $\text{So-NO}$  catalyst was almost the same. It can be concluded that different copper sources brought a profound influence on  $\text{CuAl}_2\text{O}_4$  enrichment degree.

The XPS spectra of different  $\text{CuAl}_2\text{O}_4$  spinel after the reaction were shown in Fig. 7(b). After peak fitting, the  $\text{Cu } 2p_{3/2}$  exhibited two peaks with the binding energy at 932.4 eV and 934.6 eV. Owing to the absence of shake-up satellite of  $\text{Cu}^{2+}$ , the peak located at 932.4 eV was attributed to  $\text{Cu}^+$  or  $\text{Cu}^0$ , which was further corroborated by the X-ray excited Auger electron spectroscopy spectra of  $\text{Cu LMM}$  [see Fig. 7 (c)]. The peaks at 916.7 eV and 918.8 eV were assigned to  $\text{Cu}^+$  and  $\text{Cu}^0$ , respectively (Dai et al., 2001, Faungnawakij et al., 2009, Sun et al., 2020). As shown in Table 2, there were differences in the  $\text{Cu}^+/\text{Cu}^0$  ratio on the catalyst surface, fol-

lowing the order:  $\text{So-OH} > \text{So-NO} > \text{So-O}$ , which was similar to the molar percentage of  $\text{CuAl}_2\text{O}_4$  on the catalyst surface. Thus, it can be concluded that a higher  $\text{CuAl}_2\text{O}_4$  enrichment degree favored the formation of more  $\text{Cu}^+$  on the catalyst surface. It was worth noting that the  $\text{CuO}$  reduction peak was observed in the  $\text{H}_2$ -TPR profiles of the  $\text{So-NO}$  and  $\text{So-O}$  catalysts after the reaction, but the binding energy peak of  $\text{CuO}$  did not appear in  $\text{Cu } 2p_{3/2}$ , illustrating that  $\text{CuO}$  on the catalyst surface was easy to be reduced to  $\text{Cu}^+$  or  $\text{Cu}^0$ , while  $\text{CuO}$  in the catalyst bulk was more difficult to be reduced, in other words, the  $\text{Cu}^{2+}$  mainly existed in the bulk phase. The peak located at 934.6 eV corresponded to  $\text{CuAl}_2\text{O}_4$ , indicating part of  $\text{CuAl}_2\text{O}_4$  spinel was not completely decomposed during the reaction. Moreover, the enrichment of  $\text{Cu}^+$  over the catalyst surface after the reaction caused the binding energy of the  $\text{CuAl}_2\text{O}_4$  spinel was slightly shifted towards the low binding energy (Faungnawakij et al., 2009).

### 3.7. Activity evaluation result

Fig. 8 presented the activity evaluation results of different  $\text{CuAl}_2\text{O}_4$  spinel catalysts for  $\text{CO}$  hydrogenation. The carbon

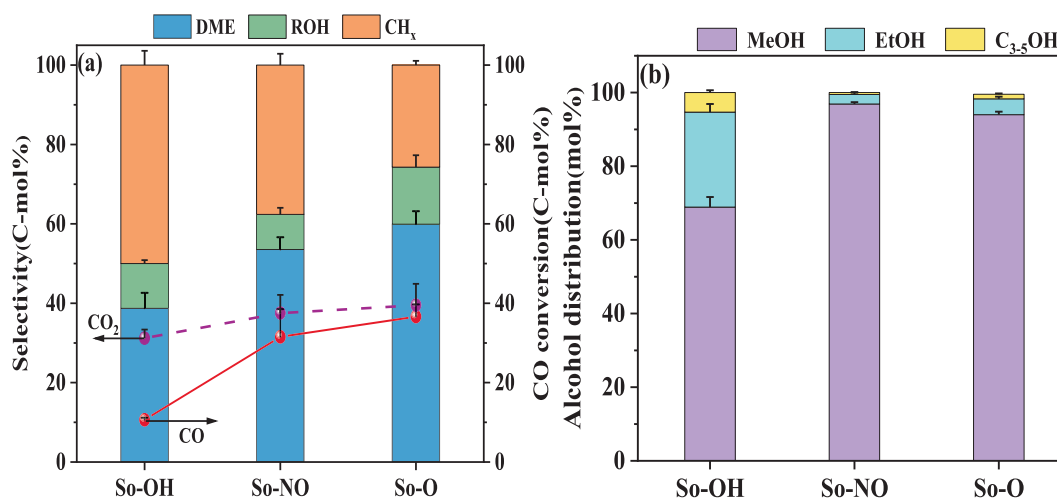


Fig. 8 CO conversion, product selectivity (a) and alcohol distribution (b) of different  $\text{CuAl}_2\text{O}_4$  spinels.

balance of all catalysts was higher than 85 %. It can be seen from Fig. 8(a) that the copper source obviously affected the catalytic activity. The CO conversion of the catalysts followed the sequence of  $\text{So-OH} < \text{So-NO} < \text{So-O}$ . Combined with XPS characterization, it was found that the higher  $\text{CuAl}_2\text{O}_4$  enrichment degree on the catalyst surface, the lower CO conversion. Moreover, more  $\text{Cu}^0$  in the catalysts resulted in higher CO conversion. The reason may be that the presence of a higher amount of free  $\text{CuO}$  on the catalyst surface can be played a role as an initiator to promote more  $\text{CuAl}_2\text{O}_4$  to be decomposed and reduced to  $\text{Cu}^0$ . The  $\text{Cu}^0$  was considered as the active site for CO activation and  $\text{H}_2$  dissociation and adsorption (Liu et al., 2017a).

Without considering  $\text{CO}_2$ , the total selectivity of dimethyl ether and alkane for the three catalysts was over 85 %. The highest selectivity of dimethyl ether reached 59.9 %, while the highest total alcohols selectivity was only 14.4 %. The selectivity of dimethyl ether followed the order:  $\text{So-OH} < \text{So-NO} < \text{So-O}$ , which was consistent with the order of the  $\text{Cu}^0$  content of the catalyst surface after the reaction. According to the above characterization, the  $\text{CuAl}_2\text{O}_4$  spinel can be decomposed and reduced to  $\text{Cu}^0$  and  $\gamma\text{-Al}_2\text{O}_3$  during the reaction.  $\text{Cu}^0$  was the active site for methanol synthesis, and  $\gamma\text{-Al}_2\text{O}_3$  was the traditional methanol dehydration catalyst. The intense interaction between  $\text{Cu}^0$  and  $\gamma\text{-Al}_2\text{O}_3$  favored the production of dimethyl ether. Moreover, with the selectivity of dimethyl ether increasing, the alkanes selectivity showed a downward trend. It was reported that the  $-\text{CH}_x\text{O}$  intermediate was formed during the CO hydrogenation, and then  $-\text{CH}_x\text{O}$  can be directly hydrogenated to methanol, which can be further dehydrated to dimethyl ether. Besides,  $-\text{CH}_x\text{O}$  can also be polarized and deoxygenated by  $\text{Cu}^+$  to form  $-\text{CH}_x$  and then hydrogenated to alkanes (Gong et al., 2012; Wang et al., 2015; Li et al., 2017). Therefore, the competitive relationship between dimethyl ether and alkanes existed.

As shown in Fig. 8(b), the alcohol distribution of the three catalysts was significantly different.  $\text{C}_{2+}\text{OH}$  fraction reached 31.1 % for the So-OH catalyst, but only 3.1 % for the So-NO catalyst. According to the literature reports, the synergistic effect of  $\text{Cu}^0$  and  $\text{Cu}^+$  promoted the synthesis of  $\text{C}_{2+}\text{OH}$  (Zuo et al., 2014; Liu et al., 2017b; Guo et al., 2022; Jia et al., 2022). The more  $\text{Cu}^+$  were favorable to polarize  $\text{C}-\text{O}$  in  $-\text{CH}_x\text{O}$ ,

making it break and increase the content of  $-\text{CH}_x$ . The  $\text{CO}^*$  generated by  $\text{Cu}^0$  activation combined  $-\text{CH}_x$  to generate  $-\text{CH}_x\text{CO}$ , and then hydrogenated to  $\text{C}_{2+}\text{OH}$ . In this work, the  $\text{Cu}^+/\text{Cu}^0$  ratio on the catalyst surface was 13.49, 10.63 and 5.06 for So-OH, So-NO, and So-O, respectively, which was not the same order for the  $\text{C}_{2+}\text{OH}$  fraction. Thus, it can be shown that the  $\text{Cu}^+/\text{Cu}^0$  ratio was not the only factor in improving the  $\text{C}_{2+}\text{OH}$  fraction. Combined with the texture characterization of the catalysts, the So-OH catalyst showed a different pore structure compared with the other two. Meanwhile, its pore volume and pore size were maximum. It was reported that the larger pore size was conducive to the diffusion of syngas, and the much more pore volume helped to reduce the space restriction and facilitate the growth of the carbon chain (Liu et al., 2012; Gao et al., 2017). It can be concluded that the catalysts with higher  $\text{Cu}^+/\text{Cu}^0$  ratio and larger pore volume and pore size favored the formation of higher alcohols.

#### 4. Conclusions

In the paper, the structure of  $\text{CuAl}_2\text{O}_4$  spinel was regulated by different copper sources using the solid-phase method. Characterization results showed that the  $\text{CuAl}_2\text{O}_4$  spinel was gradually decomposed to  $\text{CuO}$  and  $\text{Al}_2\text{O}_3$  during the reaction for CO hydrogenation. It was discovered that the  $\text{CuAl}_2\text{O}_4$  spinel structure relied highly on the copper sources. The difference in surface enrichment degree resulted in dissimilar decomposition and reduction ability of the  $\text{CuAl}_2\text{O}_4$  spinel, which will further tune the ratio of  $\text{Cu}^+/\text{Cu}^0$  and thus change the alcohol distribution of CO hydrogenation. The  $\text{CuAl}_2\text{O}_4$  spinel, selecting copper hydroxide as the copper source, possessed a large pore size and much more pore volume. Moreover, the highest enrichment degree of  $\text{CuAl}_2\text{O}_4$  spinel promoted the reducibility of the released  $\text{CuO}$ , which favored the formation of more  $\text{Cu}^+$  on the catalyst surface. Activity evaluation results suggested the higher ratio of  $\text{Cu}^+/\text{Cu}^0$  with larger pore size and pore volume was conducive to enhancing the chain growth and promoting  $\text{C}_{2+}\text{OH}$  selectivity. Meanwhile, the synergistic effect between  $\text{Cu}^0$  and  $\gamma\text{-Al}_2\text{O}_3$  improved the selectivity of dimethyl ether. In contrast, the catalysts using copper nitrate

and copper oxide as copper sources had a relatively smaller pore size and pore volume, and much more Cu<sup>0</sup> on the catalyst surface, facilitating the formation of methanol and dimethyl ether. The research of this paper will provide a new strategy to regulate the ratio of Cu<sup>+</sup>/Cu<sup>0</sup> and texture property by changing the structure of the CuAl<sub>2</sub>O<sub>4</sub> spinel, thus achieving different product distribution for CO hydrogenation.

### Declaration of Competing Interest

The authors declare that they have no known competing financial interests or personal relationships that could have appeared to influence the work reported in this paper.

### Acknowledgments

The authors are very thankful for the support from the National Natural Science Foundation of China (22078214) and Key R&D Program of Shanxi Province (201803D121043).

### References

- Agzamova, P.A., Belik, A.A., Streltsov, S.V., 2020. Structural stability of CuAl<sub>2</sub>O<sub>4</sub> under pressure. *J. Phys. Condens. Matter* 33. <https://doi.org/10.1088/1361-648X/abba68> 035403.
- Alshorifi, F.T., Alswat, A.A., Mannaa, M.A., et al, 2021. Facile and green synthesis of silver quantum dots immobilized onto a polymeric CTS-PEO blend for the photocatalytic degradation of p-Nitrophenol. *ACS Omega* 6, 30432–30441. <https://doi.org/10.1021/acsomega.1c03735>.
- Altass, H.M., Morad, M., Khder, A.-E.-R.-S., et al, 2021. Enhanced catalytic activity for CO oxidation by highly active Pd nanoparticles supported on reduced graphene oxide/copper metal organic framework. *J. Taiwan Inst. Chem. E.* 128, 194–208. <https://doi.org/10.1016/j.jtice.2021.08.034>.
- Altass, H.M., Ahmed, S.A., Salama, R.S., et al, 2022. Low temperature CO oxidation over highly active gold nanoparticles supported on reduced graphene oxide/Mg-BTC nanocomposite. *Catal. Lett.* <https://doi.org/10.1007/s10562-022-04026-y>.
- Arjmand, M., Azad, A.-M., Leion, H., et al, 2012. Evaluation of CuAl<sub>2</sub>O<sub>4</sub> as an Oxygen carrier in chemical-looping combustion. *Ind. Eng. Chem. Res.* 51, 13924–13934. <https://doi.org/10.1021/ie300427w>.
- Bahmanpour, A.M., Héroguel, F., Kılıç, M., et al, 2019. Cu–Al spinel as a highly active and stable catalyst for the reverse water gas shift reaction. *ACS Catal.* 9, 6243–6251. <https://doi.org/10.1021/acscatal.9b01822>.
- Dai, W.L., Qi, S., Deng, J.F., et al, 2001. XPS studies of Cu/ZnO/Al<sub>2</sub>O<sub>3</sub> ultra-fine catalysts derived by a novel gel oxalate coprecipitation for methanol synthesis by CO<sub>2</sub> + H<sub>2</sub>. *Appl. Surf. Sci.* 177, 172–179. [https://doi.org/10.1016/S0169-4332\(01\)00229-X](https://doi.org/10.1016/S0169-4332(01)00229-X).
- Deng, H.Y., Gao, Z.H., Li, Z.D., et al, 2019. Heat treatment of CuZnAl catalyst under high pressure to synthesize higher alcohols. *Energy Source Part A.* 47, 532–539. <https://doi.org/10.1080/15567036.2019.1692973>.
- Ding, D., Long, M., Cai, W., et al, 2009. In-situ synthesis of photocatalytic CuAl<sub>2</sub>O<sub>4</sub>-Cu hybrid nanorod arrays. *Chem. Commun. (Camb)* 6, 3588–3590. <https://doi.org/10.1039/b903865e>.
- El-Hakam, S.A., Alshorifi, F.T., Salama, R.S., et al, 2022. Application of nanostructured mesoporous silica/bismuth vanadate composite catalysts for the degradation of methylene blue and brilliant green. *J. Mater. Res. Technol.* 18, 1963–1976. <https://doi.org/10.1016/j.jmrt.2022.03.067>.
- Fan, J.C., Yang, R.Q., Zhao, J., et al, 2013. Chemical change of copper species in liquid paraffin. *Chinese J. Appl. Chem.* 30, 67–72. <https://doi.org/10.3724/SP.J.1095.2013.20044>.
- Faungnawakij, K., Shimoda, N., Fukunaga, T., et al, 2009. Crystal structure and surface species of CuFe<sub>2</sub>O<sub>4</sub> spinel catalysts in steam reforming of dimethyl ether. *Appl. Catal. B-Environ.* 92, 341–350. <https://doi.org/10.1016/j.apcatb.2009.08.013>.
- Feng, D.M., Zuo, Y.Z., Wang, D.Z., et al, 2009. Steam reforming of dimethyl ether over coupled catalysts of CuO-ZnO-Al<sub>2</sub>O<sub>3</sub>-ZrO<sub>2</sub> and solid-acid catalyst. *Chinese J. Chem. Eng.* 17, 64–71. [https://doi.org/10.1016/S1004-9541\(09\)60034-3](https://doi.org/10.1016/S1004-9541(09)60034-3).
- Gao, Z.H., Liu, Y., Li, L.L., et al, 2017. CuZnAl catalysts prepared by precipitation-hydrothermal method for higher alcohols synthesis from syngas. *Energy Source Part A.* 39, 1625–1631. <https://doi.org/10.1080/15567036.2017.1356888>.
- Gong, J.L., Yue, H.R., Zhao, Y.J., et al, 2012. Synthesis of ethanol via syngas on Cu/SiO<sub>2</sub> catalysts with balanced Cu<sup>0</sup>-Cu<sup>+</sup> sites. *J. Am. Chem. Soc.* 134, 13922–13925. <https://doi.org/10.1021/ja3034153>.
- Guo, L.N., He, X.B., Lyu, L., et al, 2022. Modulation of CuO surface properties for selective electrocatalytic reduction of CO<sub>2</sub> to HCOOH. *J. Inorg. Mater.* 37, 29–37. <https://doi.org/10.15541/jim20210547>.
- Hou, X.N., Qing, S.J., Liu, Y.J., et al, 2021. Cu<sub>1-x</sub>Mg<sub>x</sub>Al<sub>3</sub> spinel solid solution as a sustained release catalyst: one-pot green synthesis and catalytic performance in methanol steam reforming. *Fuel* 284. <https://doi.org/10.1016/j.fuel.2020.119041> 119041.
- Huang, W., Song, Y.J., Fan, J.C., et al, 2011. Effect of Si/Al ratio on the performance of Cu-Zn-Si-Al catalyst prepared by complete liquid-phase technology for dimethyl ether synthesis from syngas. *Chem. J. Chinese U.* 32, 118–123. [https://doi.org/10.1016/S1872-2067\(10\)60172-6](https://doi.org/10.1016/S1872-2067(10)60172-6).
- Jia, P.L., Liu, Y.J., Yang, R., et al, 2022. Insight into the structural sensitivity of CuZnAl catalysts for CO hydrogenation to alcohols. *Fuel* 323. <https://doi.org/10.1016/j.fuel.2022.124265> 124265.
- Kwak, B.K., Park, D.S., Yun, Y.S., et al, 2012. Preparation and characterization of nanocrystalline CuAl<sub>2</sub>O<sub>4</sub> spinel catalysts by sol-gel method for the hydrogenolysis of glycerol. *Catal. Commun.* 24, 90–95. <https://doi.org/10.1016/j.catcom.2012.03.029>.
- Li, G.J., Gu, C.T., Zhu, W.B., et al, 2018. Hydrogen production from methanol decomposition using Cu-Al spinel catalysts. *J. Clean. Prod.* 183, 415–423. <https://doi.org/10.1016/j.jclepro.2018.02.088>.
- Li, X.L., Zhang, Q.D., Xie, H.J., et al, 2017. Facile preparation of Cu-Al oxide catalysts and their application in the direct synthesis of ethanol from syngas. *ChemistrySelect* 2, 10365–10370. <https://doi.org/10.1002/slct.201701910>.
- Liu, Y.J., Deng, X., Han, P.D., et al, 2017a. CO hydrogenation to higher alcohols over CuZnAl catalysts without promoters: effect of pH value in catalyst preparation. *Fuel Process. Technol.* 167, 575–581. <https://doi.org/10.1016/j.fuproc.2017.08.012>.
- Liu, Y.J., Deng, X., Han, P.D., et al, 2017b. Higher alcohols synthesis from syngas over P-promoted non-noble metal Cu-based catalyst. *Fuel* 208, 423–429. <https://doi.org/10.1016/j.fuel.2017.07.043>.
- Liu, Y.J., Cui, N., Jia, P.L., et al, 2020a. Synergy between active sites of ternary CuZnAlOOH catalysts in CO hydrogenation to ethanol and higher alcohols. *ACS Sustain. Chem. Eng.* 8, 6634–6646. <https://doi.org/10.1021/acssuschemeng.9b07587>.
- Liu, Y.T., Deng, D.H., Bao, X.H., 2020c. Catalysis for selected C1 chemistry. *Chem* 6, 2497–2514. <https://doi.org/10.1016/j.chempr.2020.08.026>.
- Liu, J.G., Ding, M.Y., Wang, T.J., et al, 2012. Structure and performance of Cu-Fe bimodal support for higher alcohol syntheses. *Acta Phys-Chim Sin.* 28, 1964–1970. <https://doi.org/10.3866/pku.Whxb201205213>.
- Liu, J., Jia, Y.Z., Wang, S., et al, 2022a. Effect of ZnO morphology on the performance of CuZnAl slurry catalysts for the ethanol synthesis from syngas. *Fuel Process. Technol.* 238. <https://doi.org/10.1016/j.fuproc.2022.107510>.

- Liu, Y.J., Qing, S.J., Hou, X.N., et al, 2020b. Synthesis of Cu-Al spinels and its non-isothermal formation kinetics analysis. *Fuel Chem. Technol.* 48 (3), 338–348. <https://doi.org/10.3969/j.issn.0253-2409.2020.03.010>.
- Liu, Y.J., Kang, H.F., Hou, X.N., et al, 2022b. Sustained release catalysis: dynamic copper releasing from stoichiometric spinel CuAl<sub>2</sub>O<sub>4</sub> during methanol steam reforming. *Appl. Catal. B-Environ.* 122043. <https://doi.org/10.1016/j.apcatb.2022.122043>.
- Luo, M.F., Fang, P., He, M., et al, 2005. In situ XRD, Raman, and TPR studies of CuO/Al<sub>2</sub>O<sub>3</sub> catalysts for CO oxidation. *J. Mol. Catal. A-Chem.* 239, 243–248. <https://doi.org/10.1016/j.molcata.2005.06.029>.
- Maiti, S., Llorca, J., Dominguez, M., et al, 2016. Combustion synthesized copper-ion substituted FeAl<sub>2</sub>O<sub>4</sub> (Cu<sub>0.1</sub>Fe<sub>0.9</sub>Al<sub>2</sub>O<sub>4</sub>): a superior catalyst for methanol steam reforming compared to its impregnated analogue. *J. Power Sources* 304, 319–331. <https://doi.org/10.1016/j.jpowsour.2015.11.066>.
- Salama, R.S., El-Bahy, S.M., Mannaa, M.A., 2021a. Sulfamic acid supported on mesoporous MCM-41 as a novel, efficient and reusable heterogenous solid acid catalyst for synthesis of xanthen, dihydropyrimidinone and coumarin derivatives. *Colloid Surf. A.* 628,. <https://doi.org/10.1016/j.colsurfa.2021.127261> 127261.
- Salama, R.S., Mannaa, M.A., Altass, H.M., et al, 2021b. Palladium supported on mixed-metal-organic framework (Co-Mn-MOF-74) for efficient catalytic oxidation of CO. *RSC Adv.* 11, 4318–4326. <https://doi.org/10.1039/d0ra09970h>.
- Severino, F., Brito, J.L., Laine, J., et al, 1998. Nature of copper active sites in the carbon monoxide oxidation on CuAl<sub>2</sub>O<sub>4</sub> and CuCr<sub>2</sub>O<sub>4</sub> spinel type catalysts. *J. Catal.* 177, 82–95. <https://doi.org/10.1006/jcat.1998.2094>.
- Sickafus, K.E., Wills, J.M., Grimes, N.W., 1999. Structure of spinel. *J. Am. Ceram. Soc.* 82, 3279–3292. <https://doi.org/10.1111/j.1151-2916.1999.tb02241.x>.
- Sun, Y.K., Zeng, J.M., Zhang, J., et al, 2020. Combustion products of calcium carbide reused by Cu-based catalysts for acetylene carbonylation. *ACS Omega* 5, 27692–27701. <https://doi.org/10.1021/acsomega.0c04289>.
- Wan, Y., Zhou, Z., Cheng, Z., 2016. Hydrogen production from steam reforming of methanol over CuO/ZnO/Al<sub>2</sub>O<sub>3</sub> catalysts: Catalytic performance and kinetic modeling. *Chinese J Chem Eng.* 24, 1186–1194. <https://doi.org/10.1016/j.cjche.2016.02.006>.
- Wang, Y., Shen, Y.L., Zhao, Y.J., et al, 2015. Insight into the balancing effect of active Cu species for hydrogenation of carbon–oxygen bonds. *ACS Catal.* 5, 6200–6208. <https://doi.org/10.1021/acscatal.5b01678>.
- Wang, Y.Q., Xue, R., Zang, M., et al, 2017. Spinel AFe<sub>2</sub>O<sub>4</sub> catalysts: Preparation and catalytic combustion of toluene. *J. Inorg. Mater.* 32, 1068–1074. <https://doi.org/10.15541/jim20160705>.
- Xi, H.J., Li, G.J., Qing, S.J., et al, 2013. Cu-Al spinel catalyst prepared by solid phase method for methanol steam reforming. *J. Fuel Chem. Technol.* 41, 998–1002. <https://doi.org/10.3969/j.issn.0253-2409.2013.08.015>.
- Xi, H., Hou, X., Liu, Y., et al, 2014. Cu-Al spinel oxide as an efficient catalyst for methanol steam reforming. *Angew. Chem. Int. Ed. Engl.* 53, 11886–11889. <https://doi.org/10.1002/anie.201405213>.
- Yan, P.Q., Wang, J.R., Shen, Y.X., et al, 2021. Effect of CuAl<sub>2</sub>O<sub>4</sub> spinel structure on CO hydrogenation in slurry reactor. *Chem. J. Chinese U.* 42, 1846–1854. <https://doi.org/10.7503/cjcu20200883>.
- Yong, S.T., Ooi, C.W., Chai, S.P., et al, 2013. Review of methanol reforming-Cu-based catalysts, surface reaction mechanisms, and reaction schemes. *Int. J. Hydrogen Energy* 38, 9541–9552. <https://doi.org/10.1016/j.ijhydene.2013.03.023>.
- Zuo, Z.J., Wang, L., Yu, L.M., et al, 2014. Experimental and theoretical studies of ethanol synthesis from syngas over CuZnAl catalysts without other promoters. *J. Phys. Chem. C* 118, 12890–12898. <https://doi.org/10.1021/jp502828c>.